



**Proceedings of the Sixth International Conference on
Asian and Pacific Coasts (APAC 2011)**

December 14 – 16, 2011, Hong Kong, China

**THREE-DIMENSIONAL NUMERICAL STUDY ON BORE
DRIVEN SWASH**

B. DENG, C.B. JIANG, L.P. ZHAO

*School of Hydraulic Engineering, Changsha University of Science & Technology,
Changsha 410004, P.R.China*

*Hunan Province Key Laboratory of Water, Sediment Sciences & Flood Hazard
Prevention, Changsha 410004, P.R.China*

H.S. TANG

*School of Hydraulic Engineering, Changsha University of Science & Technology,
Changsha 410004, P.R.China*

Department of Civil Engineering, The City college of New York, New York 10031, USA

The dynamics of flow involved with surge bore propagating over a slope is studied numerically using a fully three-dimensional (3D), incompressible, two-phase flow Navier-Stokes (NS) solver coupled to a LES turbulence model. A high-resolution STACS-VOF method is applied to capture the interface between the air and water phases. The computed uprush shoreline motion and the tip of runup water surface compare favorably with experimental data. Numerical results are also presented for the instantaneous flow field, recirculation regions, vortex tubes, and maximal bed shear stress. The results indicate that the flow phenomena are very complicated after the bore breaks.

Key words: Swash zone; Bore; Two-phase flow; Bed shear stress;

1. Introduction

The swash zone is the cross-shore region of beach covered by flow uprush and flow backwash following wave breaking [1], where waves dissipate or reflect their energy when traveling towards the sea shore [2]. Breaking waves in the surf zone and wave run-up in the swash region play an important role in coastal engineering since they are the driving forces for various nearshore phenomena, such as coastal erosion [3,4], wave-structure interaction [5,6], sediment transport and morphodynamics[7-9]. Swash hydrodynamics are characterized by fluid uprushes and backwashes on the beachface. Therefore, it is essential to analyze the generation and evolution of bores in swash zones to understand the characteristics of hydrodynamics on beach [10].

Great progress has been made in measurements [1,11,12], numerical modeling using Reynolds Averaged Navier-Stokes (RANS) solvers [13,14], yet the small scale flow characteristics in this region are still poorly described. Most numerical models are used to test the model's ability to approximate wave

breaking, run-up and overtopping. However, these results indicate that swash flow is almost consistent over depth and these models can't satisfactorily describe flows in bore collapse, uprush and backwash phase. Simulation results for free surfaces should be improved, especially the sheet flow with air entrainment formed during the swash process. Meanwhile, most of them are 1D or 2D numerical models unable to well describe swash flows' three-dimensional feature which, according to Yeh [12], is very important to understand swash flow hydrodynamics.

This study aims to achieve an accurate and complete understanding of hydrodynamic characteristics of swash zones, which are studied numerically using a fully three-dimensional incompressible two-phase flow Navier-Stokes (NS) solver, coupled to LES turbulence model and a High-resolution STACS-VOF method, with good accuracy in describing air/water surfaces. Based on the results obtained from the numerical simulations, details of hydrodynamics after bore breaking are presented.

2. Model Description

2.1. Governing Equations

For the incompressible viscous flows of two immiscible fluids with constant properties, the Navier-Stokes equations are given as follows:

$$\frac{\partial \rho U}{\partial t} + \rho U \cdot \nabla U = -\nabla p + \nabla \mu S + F \quad (1)$$

$$\nabla \cdot U = 0 \quad (2)$$

Where, ρ is the density, t is time, U is the velocity, p is pressure, μ is the dynamic viscosity coefficient, F is the body force, including gravity and surface tension. After filtering the governing equations, the Reynolds stresses are expressed using a turbulence closure model, the widely used LES-SGS model in this paper (see Smagorinsky [15] for an overview).

2.2. Interface Capturing

The VOF method can be used to track the interface of two immiscible fluids.

$$\frac{\partial C}{\partial t} + U \cdot \nabla C = 0 \quad (3)$$

In the above equations, C is the volume fraction, which is defined as: (1) $C=1 \Rightarrow$ control volume is filled only with phase 1 (water), (2) $C=0 \Rightarrow$ control volume is filled only with phase 2 (air), (3) $0 < C < 1 \Rightarrow$ interface present. The local densities and viscosities are functions of the fluid to which they are related:

$$\rho = \rho_1 + C(\rho_1 - \rho_2) \quad (4)$$

$$\mu = \mu_1 + C(\mu_1 - \mu_2) \quad (5)$$

The Crank-Nicolson differencing scheme is used for temporal discretization. The scheme developed by Darwish, et al. named STACS (Switching Technique for Advection and Capturing of Surfaces) is employed in this work [16]. STACS is a high resolution scheme based on the Normalized Variable Diagram (NVD). It is generally recognized that predications obtained from the STACS scheme are far more accurate and less diffusive preserving interface sharpness and boundedness at all Courant number values considered.

2.3. Numerical Methods

The finite volume method is used to discretize the governing equations together with a block structure grid system. In computation, the SIMPLE (Semi-Implicit Method for Pressure-Linked Equations) is adopted, where the second-order central difference scheme is used for the diffusion terms while the second-order upwind difference scheme is employed to approximate the convection terms. Meanwhile, with algebraic multi-grid method (AMG), linear system of equations is solved, and the flow solver is parallelized by domain decomposition using OpenMP.

3. Setup

Yeh et al. studied experimentally bore collapse and runup over a uniform slope [12]. The dam-break mechanism is used to generate bores in a region with constant depths. A definition sketch for the experimental setup is shown in Figure 1. The water depth in front of the dam (gate) was h_1 and the water depth behind it h_0 . The gate at X_{gate} was pulled instantaneously and the resulting bore ran up a slope of $\beta=7.5^\circ$. The parameters value in this study is the same with this experimental setup as follows: $h_1=22.52\text{cm}$, $h_0=9.75$, $X_{gate}=a=297\text{cm}$, $b=40\text{cm}$. Meanwhile, the computational region is depicted in Figure 1. It is 679cm long (It is enough to ensure water unable flowing out from the right side), 30cm wide and 70cm high, and the whole computational region is divided to two blocks. The total number of grid nodes is approximately 2.2 million. The symmetry boundary conditions are applied at $z=70\text{cm}$ and at the North (South) side. No-slip conditions are specified on the left (right) and the bottom solid wall.

In reality, the beach configuration is complex. We will not pursue this issue in this paper so as to focus on the physical processes in swash flows. Before studying a bore running up the slope, it is important to make sure that the numerical model can generate the bore correctly through the dam-break mechanism. The verification of the numerical model for the bore generation on a flat bed has been shown in our previous work (see [17]) and will not be repeated here.

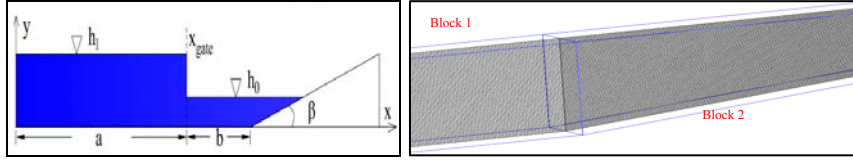


Figure 1. Sketch for the experimental setup (left), Computational domain and block-structure grid layout (right).

4. Results and discussions

4.1. Model Validation

First, the numerical model is validated with experimental data presented by Yeh et al. [12]. Figure 2. shows a sequence of photographs comparisons between the numerical and experimental results for the run-up waterline near its maximum. It is seen that the simulation results are in good agreement with the experimental results. As is seen, the waterline is not straight, but instead forms distinct ‘tongues’ and it demonstrates an obvious three-dimensional feature (also see Figure 3.). The tongue formations must be due to the air-water-beach contact-line effects [12]. Figure 2 also shows the formation of complex capillary waves as well as the formation of ridges behind the waterline. We can't get such characteristics in two-dimensional numerical simulation. Yeh interpreted that the ridge formation is generated by irregularities of the bore front. Turbulent rollers on the bore front are irregular and three-dimensional, and the turbulence is advected onto the beach during the transition process at the shoreline. These irregularities at the shoreline may influence the formation of a run-up water sheet [12]. Computation simulating the appearance of the successive run-up motion successful is also observed and it must be relative to the transition process at the shoreline.

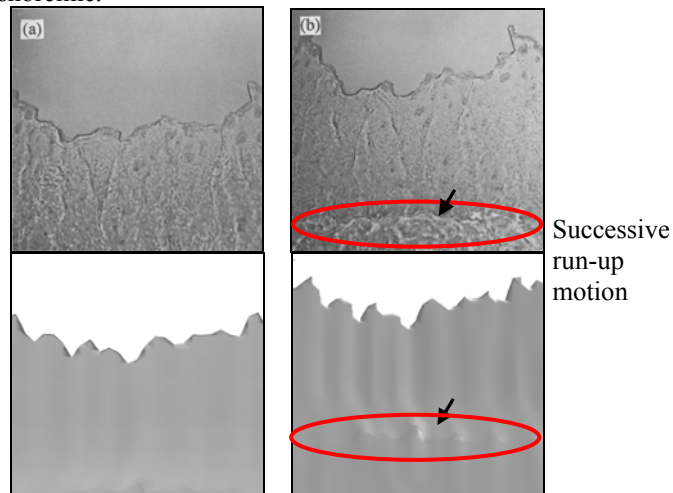


Figure 2. The run-up waterline near its maximum predicted by numerical model and experimental data by Yeh [12]. (a): $T=2.4s$ and (b): $T=2.7s$.

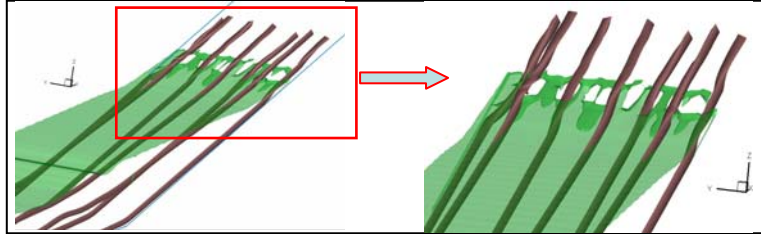


Figure 3. Vortex tube and instantaneous fraction contours of the free surface.

Figure 4 shows the evolution of bore heights for the bore during the shoaling process. To correspond to the result of Zhang [14], we conduct a dimensionless coordinate both in the spatial and temporal coordinates as Zhang's work. It is interesting to observe that the theoretical NSW results (Ho and Meyer [18]) agree with the bore height measured behind the bore head quite well away from the still-water shoreline. The NSW theory predicts that the bore height diminishes to zero at the still-water shoreline. However, experimental data and present numerical results show that the bore heights remain constant over most of the shoaling process. In reality the bore front becomes much more aerated when it breaks near $x=0$. Numerical results by Zhang *et al.* fall noticeably below the experimental results near the still-water shoreline, for they ignored trapped air bubbles when extracting the bore height information from the volume fraction results, and thus failed to model the detailed evolution of the air–water mixture. In our study, we set up a gas–liquid two phase flow model, in which the interaction between air and water was considered; therefore, the bore heights of our numerical results are consistent with the experimental results near the still-water shoreline.

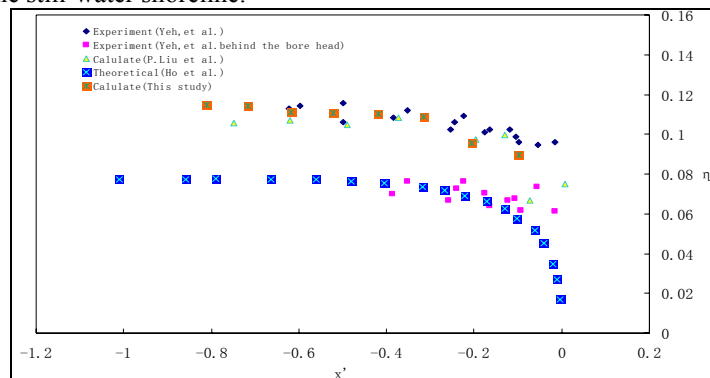


Figure 4. The evolution of bore heights for the bore during the shoaling process.

4.2. Instantaneous Flow Field

After the bore breaking, the bore front collapses onto the beach and loses its steep free surface profile, and then the uprush and backwash come into being. Four snap shots of the uprush or backwash's motion process in the transitional period (between uprush end and backwash beginning), in terms of instantaneous flow field, ensemble free surface profile and streamlines are shown in Figure 5.

As the water tongue moves landwards, the effects of bottom stress accumulate and the water particles close to the beach face travel noticeably more slowly than those near the free surface (Figure 5(a)). On the other hand, because of longer exposure to bottom friction and gravity, fluid particles near the tip of runup tongue move at a slower speed than those in the rear of the water tongue. When the bore runup reached to the maximum runup height, part of water column under the water tongue will begin to move in the opposite direction and the flow velocity reached minimum. From the same Figure, we also notice a series of small vortexes appear under the water tongue, which consume the energy of flow gradually. That's a reason why the uprush moves slowly in the late runup process.

The backwash is formed when the uprush reaches to the maximum runup height by the gravity force. At the beginning of the backwash, the backwash velocity is relatively small, but the flow characteristics on the beach are very complicated. As shown in Figure 5(b), the flow in the vicinity of shoreline first change its direction of motion and start to move seaward, while the rest of bore is still propagating shoreward because of the remaining shoreward kinetic energy during the runup process. These two opposite currents interact violently with each other, generating a long, narrow recirculation region. On the seaward side of the bore, the velocity profiles show strong variations in all directions. The backwash velocity is increasingly faster by the gravity force after an interval, and then the front water of shoreline move reversely. As the backwash gradually increases, the vorticity centre move down slightly and close to the surface. With above analysis, uprush and backwash interact violently during this transitional period.

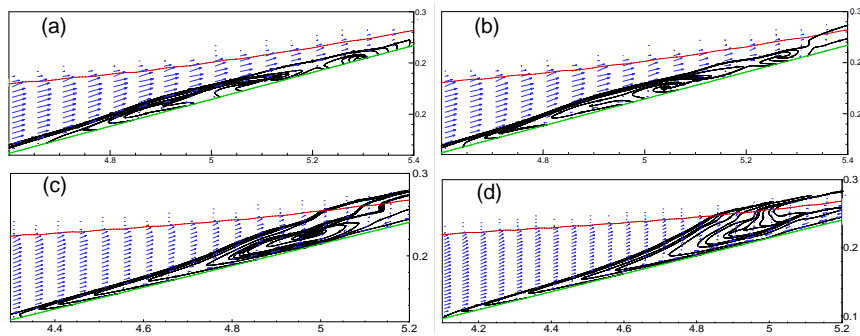


Figure 5. The instantaneous flow field.

Figure 6 indicates the spatial variation of recirculation regions. In the Figure, there are two recirculation regions. We define one mainly caused by uprush as 1#, while the other one mainly caused by backwash as 2#, both of which located at the center of the vortex. It shows that, during this transitional period, the recirculation region's range is increasing, but the size of 1# is less

than that of 2#. When the process of backwash completely starts, these two recirculation regions should be merged, but the center position locate in the proximity of $x=5\text{m}$ all the time, so it is likely that there is movement of pushed and suspended sediments which leads to beach evolution.

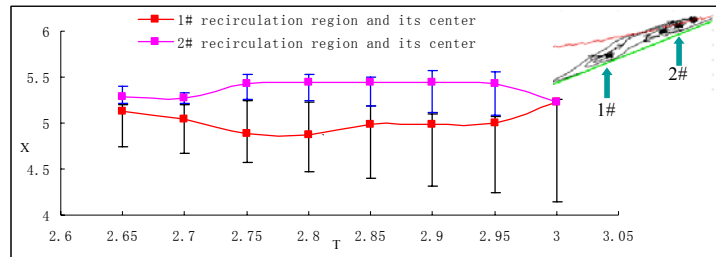


Figure 6. The evolution of bore heights for the bore during the shoaling process.

4.3. The Maximal Bed Shear Stress

Typical time histories of fluid trajectories, the position and its value of the calculated maximal bed shear stress are shown in Figure 7. The fluid trajectories show that all the flow acceleration during the uprush occurs seaward of, or very close to, the SWL, and it may be expected to result in a thin boundary layer as the initial condition at the start of the uprush [19]. Meanwhile, results show that there is a transient accelerated movement both in bore runup or rundown process and when the bed shear stress increases rapidly. The bore runup reaches to the maximum height at about $t=2.7\text{s}$, and the rundown moves slowly in later period.

Figure 7 also indicates strong temporal and spatial variation in the maximal bed shear stress throughout the swash cycle; it has rapid temporal variation through the leading edge of the uprush and a clear distinction between the uprush and backwash phase, but the maximum bed shear stress locates nearby the place at $x=5\text{m}$ in this transitional period. For a single swash event, the results show that the maximum shear stress at the leading edge of the swash is usually 2-4 times greater than the maximum bed shear stress in the backwash; it is similarly reported by Barnes [20].

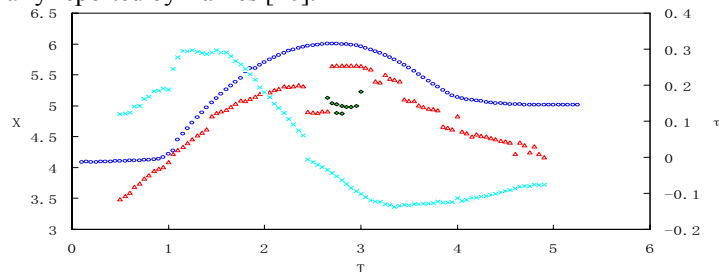


Figure 7. The position of runup (\circ) and The center of recirculation region (\blacklozenge); The position and its value of the maximal bed shear stress (\triangle , \times)

5. Conclusions

In this paper, a new numerical model is produced with detailed prediction of hydrodynamics within swash generated by bore collapse on a beach. The computed uprush shoreline motion and the tip of runup water surface compare favorably with experimental data. Meanwhile, results are presented for instantaneous flow field, the characteristics of recirculation region (from the end of runup to the beginning of rundown), vortex tube and the maximal bed shear stress. The results show that the flow characteristics on the beach are very complicated after the bore breaks, especially in the transitional period between uprush end and backwash beginning. There are many small-scale vortices near the beach and the vortex tube demonstrates an obvious three-dimensional feature. The center of recirculation region and the maximal bed shear stress encounter during the same transitional period and in the same region.

Acknowledgments

The study was supported by the National Natural Science Foundation of China (No.51179015, 50979008, 41176072), the Ph.D. Programs Foundation of Ministry of Education of China (20094316110002). B. Deng is Supported by Hunan Provincial Innovation Foundation For Postgraduate. H. S. Tang is supported by PSC CUNY

References

1. T. O'Donoghue, D. Pokrajac, et al, *Coast. Eng.* **57**, 513 (2010).
2. M. Larson, S. Kubota, L. Erikson, *Mar Geol.* **212**, 61 (2004).
3. A.H. Sallenger, W. Krabill, J. Brock, et al, *Mar. Geol.* **187**, 279 (2002).
4. M. Larson, L. Erikson, H. Hanson, *Coast. Eng.* **51**, 675 (2004).
5. D.H. Peregrine, S.M. Williams, *J. Fluid Mech.* **57**, 513 (2001).
6. P.L.F. Liu, K. Al-Banaa, *J. Fluid Mech.* **505**, 225 (2004).
7. B. Elfrink, T.E. Baldock, *Coast. Eng.* **45**, 149 (2002).
8. T.E. Baldock, M.G. Hughes, K. Day, J. Louys, *Coast. Eng.* **52**, 633 (2005).
9. G. Masselink, , J.A. Puleo, *Cont. Shelf Res.* **26**, 661 (2006).
10. R. Bakhtyar, D.A. Barry, et al, *Adv. Water Resou.* **32**, 250(2009).
11. M. Petti, and S. Longo, *Coast. Eng.* **43**, 1(2001).
12. H.H. Yeh, A.Ghazali, I.M. Marton, *J. Fluid Mech.* **206**, 563(1989).
13. J. Puleo, A. Farhadzadeh, and N. Kobayashi, *J. Geophys. Res.* **112**, (2007).
14. Q. Zhang and P.F. Liu, *Coast. Eng.* **55**, 1113(2008).
15. J.Smagorinsky, *Mon. Wea. Rev.* **91**, 99(1963).
16. M. Darwush, F.Moukalled. *Num. Hea. Tra. B.* **49**, 19(2006).
17. B. Deng, C.B. Jiang, et al. *CJ JOINT.* 472(2010).
18. D.V. Ho, R.E. Meye, *J. Fluid Mech.* **14**,305(1962).
19. E.A. Cowen, I.M. Sou, P.L.F. Liu, et al., *J. Eng. Mech.* **29**, 1119(2003).
20. M. P. Barnes, T. E. Baldock, *J. Coast. Res.* **SI50**, 641(2007).